Anisotropy in turbulence profiles of stratified wakes

G. R. Spedding

Citation: Phys. Fluids **13**, 2361 (2001); doi: 10.1063/1.1383784
View online: http://dx.doi.org/10.1063/1.1383784
View Table of Contents: http://pof.aip.org/resource/1/PHFLE6/v13/i8
Published by the American Institute of Physics.

Anisotropy in turbulence profiles of stratified wakes

G. R. Spedding[a)]
Department of Aerospace and Mechanical Engineering, University of Southern California, Los Angeles, California 90089-1191

(Received 22 November 2000; accepted 15 May 2001)

At sufficiently high values of the Reynolds number ($Re \geqslant 4.5\times 10^3$) and internal Froude number ($F \geqslant 4$), initially turbulent bluff body wakes evolve in the presence of a stable background density gradient with wake-averaged mean and turbulence length and velocity scales that are independent of Re and F for at least two orders of magnitude extension in both parameters. The way in which the initially three-dimensional motions transition to the characteristic (and Re- and F-independent) late wakes (where vertical velocities, $w \ll u,v$) is both of great practical interest, and complex, hence somewhat unclear. Here, digital particle imaging velocimetry type measurements on towed-sphere wakes are described, so that the development of anisotropy can be measured by the time development of turbulence profiles in horizontal and vertical centerplanes. The observed anisotropies can be associated with energy transfer to internal wave modes, and suppression of other vertical displacements, that contrasts with sphere wakes at similar Re in a homogeneous fluid. Maximum Reynolds stresses occur at the boundary of a sinuous undulation of the wake, which increases in amplitude up to $Nt \approx 60$ (N is the buoyancy frequency that characterizes the strength of the stratification). Although an intrinsic wake profile instability cannot be excluded, the observed wake element spacings can be accounted for by known spiral and Kelvin–Helmholtz instabilities in the near wake. © *2001 American Institute of Physics.* [DOI: 10.1063/1.1383784]

I. INTRODUCTION

A. Characteristics of stratified wakes

Meteorological (flow over islands, sea-mounts) and naval (submarines) applications of stratified wakes research frequently involves flows at high Reynolds number ($Re = UD/\nu$, for a body of diameter, D, traveling at speed, U, through a fluid with kinematic viscosity, ν). By contrast, characteristic values of the internal Froude number ($F = 2U/ND$, where N is the buoyancy frequency in rad/s) range from 10^{-1} to 10^3, and the comparative importance of buoyancy forces might be expected to vary accordingly. However, even when initial values of F are high, as the wake turbulence is allowed to decay, local velocity scales decrease while corresponding integral length scales increase, and so eventually $F_{\mathrm{loc}} = O(1)$, regardless of its initial value, and buoyancy forces predominate. (F_{loc} can be based on U_0 or a fluctuating velocity magnitude, q, and with length scales in horizontal (L_H) or vertical (L_V) as appropriate; the foregoing remark applies to all cases.) The strongly stratified limit is a condition to which many episodic or intermittent turbulent flows in the ocean or atmosphere are attracted, and it has received significant attention in the research literature (see reviews by Lin and Pao,[1] Hopfinger,[2] and Riley and Lelong[3]).

Experiments on towed spheres[4,5] show that the scaling of mean and turbulence quantities in the late wake ($Nt > 100$) is independent of the initial, body Froude number over a broad range of conditions ($F \geqslant 4$, $Re \geqslant 4.5\times 10^3$). The late wake itself is characterized by the slow evolution of large patches of vertical vorticity, whose dynamics are quite consistent with the strongly stratified (low-F) analysis of Riley, Metcalfe, and Weissman.[6] Once formed, they are remarkably persistent and stable. No such large-scale structures survive in a homogeneous fluid, and the relatively ordered structure of the stratified wakes and their correspondingly high-energy densities are in sharp contrast to the normal evolution of turbulent, axisymmetric wakes.

B. The importance of the NEQ régime

The distinguishing characteristics of stratified wakes emerge in a nonequilibrium (NEQ) régime where the initially three-dimensional turbulence decays and adjusts to the continuing forcing due to the stable background density gradient. There is an evolving balance between buoyancy-induced motions and the decaying turbulence, and energy is exchanged between vortex and wave modes, while potential energy can be both created, and returned back to kinetic energy of the turbulent and/or mean flow. It is in this régime that the geometry of the final (almost) time-invariant late-wake is determined, and where the flow transitions from an isotropic [three-dimensional (3D)] turbulence to one that is so constrained by the density gradient that the vertical velocity component (w, opposed to gravity) is almost zero.

The presence of some such NEQ régime has been argued[5] to be a general characteristic of all spatially limited patches of decaying turbulence in a stably stratified ambient, because the underlying physical principles are themselves very general. Nevertheless, it is perhaps the least-well understood phase of the wake evolution. This is due, at least in

a)Telephone: (213) 740-7182. Electronic mail: geoff@usc.edu

part, to the continued importance of vertical motions (w) thus eliminating the simplifications of many investigative systems, both experimental and analytical. At the same time the constraining effects of the buoyancy forces cannot be ignored and isotropy cannot be assumed over all scales.

C. The development of anisotropy

Existing velocity field measurements[4,5,7,8] (reviewed by Spedding[9]) have tended to concentrate either on the topology or spatial distribution of vorticity components in horizontal or vertical interrogation planes, or on wake-averaged mean flow or turbulence quantities. Mean flow profiles have been shown to be self-similar, and Gaussian[4] in shape over most readily accessible times in the wake evolution, but hitherto there has been no examination of wake turbulence profiles in the NEQ (or any other) régime, and there are no comparable profiles in the literature.

The objective of this paper is to give a quantitative description of the development of mean turbulence profiles in a stratified wake. The profile shapes can be related to the physical characteristics that are unique to stratified flows, and the initial transition from three-dimensional turbulence to strongly constrained, almost (but not) two-dimensional motion can be traced in the profile evolution. The experimental resolution in time and in space has been carefully matched with the known physics of the NEQ régime. The focus will be almost exclusively on the particular case of $F=4$, which can be shown to possess all of the general characteristics of the initially turbulent (and F-independent) stratified wakes, while retaining the highest degree of repeatability and predictability for coherent and intelligible statistics. Early efforts at direct numerical simulations (DNS) and large eddy simulations (LES) of the stratified wake problem are just appearing,[10,11] and the turbulence profiles reported here can act either as a diagnostic for quantitative comparisons, or for guiding the selection of initial conditions in numerical schemes.

II. LABORATORY EXPERIMENTS

Experiments were conducted in a 2.44 m^2 tank with extended startup section, as previously described,[4] and shown in Fig. 1. Rigorously filtered water was linearly stratified with salt in a standard two-tank arrangement. Experiments with physical parameters given in Table I were conducted and analyzed for this study. The top two rows show conditions for $F=4$, and all the data shown here come from these experiments. The data for $F=16$ were used as a qualitative check for application to larger F. The tank depth, $H=24$ cm and so the ratio $D/H\in[0.106,0.212]$ is not very small. Nevertheless, its unimportance in the quantities discussed here can be verified by comparisons between rows in Table I. The rather small variation in Re is also unimportant. The insensitivity of mean and turbulence velocities in the wake to variations in Re and D/H in this range was noted in previous systematic investigations in the same apparatus.[4,5] The wire suspension to the sphere body is thin ($d=0.025$ cm) and under high tension to minimize vibration normal to the suspension plane. Step motor controlled motion is synchronized

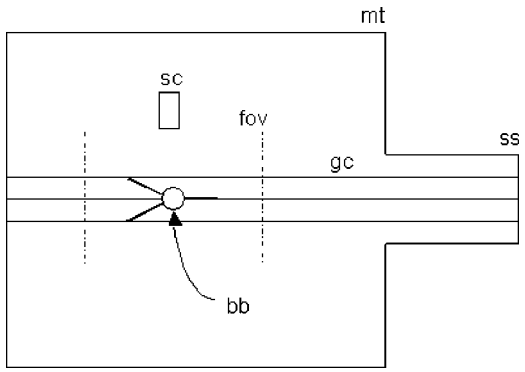

FIG. 1. Plan view of the experimental apparatus. The sphere (bb) is towed horizontally from right to left in a square tank with extended startup section (ss). The main tank (mt) is 2.44 m on a side. Data are taken, either in an isopycnal plane over the window (fov) shown by dashed lines, or in vertical planes observed by submerged camera (sc). The sphere is suspended and towed by obliquely mounted stainless steel wires under tension from supports at the guide cables (gc).

with data acquisition from a Pulnix TM9701 camera with digital output at a resolution of 768×484 pixels.

The camera is placed in either one of two positions: (i) directly above the tank, imaging a rectangular area labeled [fov] in Fig. 1, or (ii) in a submerged box off the centerline. In position (i) the tank is seeded with iso-density polystyrene beads ($d\approx0.8$ mm), marking a horizontal sheet. The isopycnal is deformed during the course of the experiment, and returns to its original position, as the mixing is quite low in each experiment. In all experiments reported here, the horizontal bead sheet is at the sphere centerplane ($z=z_0$).

The field of view is offset towards the end of the sphere travel to avoid contamination by parts of the flow field affected by startup conditions or nonuniformities in the startup-main tank junction. The forward-most position is limited by contamination from distortion of the wake as it continues to collide with the stationary sphere at the end of the experiment. Both limit conditions can be readily observed in streamwise variations in the vertical vorticity distribution, and their simultaneous intrusion (assured by the correct placement of [fov]) into the measurement volume terminates the time series analysis of the experimental data. Up until this time, the measured quantities can be verified to be unaffected, and indeed most statistical measures are surprisingly robust to this error source.

In position (ii) the entire tank is seeded with plastic-encapsulated rhodamine particles ($d\approx0.8\mu$m). Particles are introduced at the surface and allowed to drift down slowly over 2 hours. Vertical plane illumination is then provided by a laser sheet generated by a scanning mirror suspended

TABLE I. Physical parameters for towed-sphere experiments.

D (cm)	U (cm/s)	N (rad/s)	Re	F
5.08	15.4	1.51	7794	4.0
3.81	12.8	1.68	4857	4.0
2.54	26.6	1.31	6728	16.0

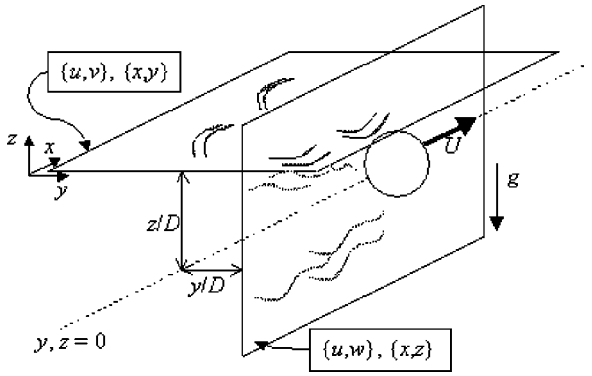

FIG. 2. Coordinate system and velocity components measured on horizontal and vertical planes in the stratified wake.

above the water surface. Although the vertical sheet can be moved, all data described here come from vertical centerplane ($y=y_0$) cuts.

The submerged camera box is about 1 m from the centerline. The earliest practical data acquisition time is limited by density field disturbances where refractive index gradients cause apparent particle image displacements at the sensor. The gradients can only be computed if the velocity field is exactly known (and even then must be integrated along the entire curved light ray path) and so a statistical criterion is used based on apparent root-mean-square displacements of particles glued to a stationary vertical black board. Experiments are conducted in identical conditions to the real thing, except without particles, and the earliest valid data analysis can occur when real experimental rms values exceed control values by a factor of 10. The physical disturbance from the camera box does not affect the measurements (as determined by horizontal plane measurements in the presence of an unoccupied camera box) before earlier constraints due to internal wave reflections and/or insufficient statistical convergence from sampling large structures in a small observation box.

The vertical slice observation box has typical size $\Delta X/D, \Delta Y/D = \{2.2, 1.6\}$, while the horizontal plane data are typically in a window of $\Delta X/D, \Delta Y/D = \{21, 13\}$. In both cases data acquisition begins as soon as the sphere leaves the observation box, and the time origin is set at the time when the sphere is at the center of the field of view. The startup section assures that the minimum travel distance before data acquisition $X_0/D \geqslant 42$.

III. ANALYSIS OF VERTICAL–HORIZONTAL SLICES

A. Estimation of velocity fields

The average displacement of groups of particles in small subrectangles was computed according to programs based on the correlation imaging velocimetry (CIV) techniques in Fincham and Spedding.[12] u, v, w velocity components are available on separate vertical and/or horizontal planes as shown in Fig. 2. Two special concerns merit further discussion.

While horizontal plane (more accurately isopycnal plane) data acquisition, calculation and analysis profit from the primarily horizontal motions of late-wakes, the same anisotropy assures that the magnitude of cross-plane motion in vertical slices will be of the same order as horizontal displacements, and (eventually) an order of magnitude larger than vertical components. Consequently, effective exposure times (δt) must be small compared with the average particle transit time across the lateral thickness of vertical sheet (or slab, $d \approx 4$ mm). The small δt leads to small displacement magnitudes, and errors that are constant in units of pixels will be a larger fraction of the total. The major limiting factor in the error of estimating small displacements is the peak-locking error[12] and particular care must be taken to minimize it. The correlation peak location is not in fact a simple spline fit, but is a nonlinear fit of the smoothing spline interpolation of individual autocorrelation functions from both source and destination image subrectangles. The effect is to increase the random noise component which, nevertheless, is decorrelated from the peak-locking error. The resulting small-scale noise can then be removed by appropriate spectral filtering (a fourth-order, Butterworth low-pass filter) provided the noise and data are well separated in length scale. The comparatively high magnification of the vertical slice data, where a typical effective grid resolution is 2×2 mm makes this approach possible.

The second major concern is in correctly distinguishing measurement errors from root-mean-square (rms) measures (for example) of purported turbulence quantities. There is no rational way of doing this, except by sufficiently conservative smoothing and–or filtering techniques that isolate known noise wave numbers or lengthscales at the possible expense of aliasing errors. The CIV method always involves a smoothing spline interpolation to correct for finite displacements off the original rectangular calculation grid. The free smoothing parameter ρ_s is usually adjusted so that peak velocities are guaranteed to be within 5% of their original, measured value, and gradient quantities are within 10% over the scales of interest. Figure 3 shows four instantaneous (not spatially averaged) streamwise velocity profiles with original and interpolated curves. In the wake defect itself, the curve adheres closely to the original data, satisfying the 5%–10% criterion. In the far field, where $|\mathbf{u}|$ is small, small scale fluctuations are presumed to be peak-locking errors and are removed successfully for $Nt \leqslant 15$. At later times, qualitatively similar variations are not completely removed, but may be damped significantly. The smoothing and filtering scheme is designed to retain all fluctuations that unambiguously belong to the flow, together with far-field fluctuations that can be attributable to internal waves. The cost of such an approach is a nonzero noise floor on any single fluctuating velocity component. All of the measurements reported here in Figs. 8–11 are averaged over ΔX of the observation window, and so the profile shapes will be unaffected because the measurement error is uncorrelated in the x direction. The absolute values, on the other hand, may be over-estimated by 5%. For $F=4$, averaging over $\Delta X/D$ is equivalent to a time average over $\Delta Nt = \frac{1}{2}\Delta X/D$.

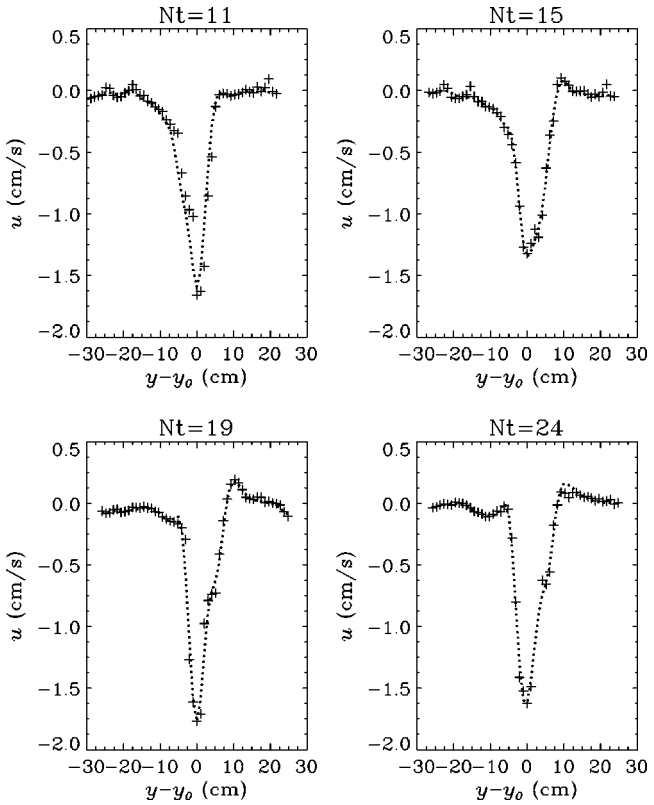

FIG. 3. Four velocity profiles taken at the arbitrary location, $\Delta X/2$, at $Nt=\{11,15,19,24\}$. The original data points are shown by + symbols, and the spline-interpolated fit is shown by the dotted line. y_0 is defined locally by the velocity minimum.

B. Notation and derived quantities

$u,v(x,y)$ and $u,w(x,z)$ fields are estimated on discrete, square grids of approximately 1 and 2 mm mesh size, respectively. The grid itself is arbitrarily defined, because spline interpolating coefficients allow for calculation of velocities and their spatial derivatives at any location inside the original data domain, but the spacing is chosen to respect the original sampling resolution. For horizontal and vertical slices, the out-of-plane (normal) vorticity components are

$$\omega_z=\frac{\partial v}{\partial x}-\frac{\partial u}{\partial y},$$
$$\omega_y=\frac{\partial w}{\partial x}-\frac{\partial u}{\partial z}. \tag{1}$$

A mean wake profile can be defined by averaging u over the streamwise length of the observation window, ΔX, and if U_X is this mean component, then in vertical slices (for example) the remainder is denoted

$$u'(x,z)=u(x,z)-U_X(z), \tag{2}$$

and similarly in the horizontal plane. The root-mean-squares are

$$u'_X(z)=\left(\frac{1}{\Delta X}\int_0^{\Delta X}u'^2(x,z)dx\right)^{1/2},$$
$$v_X(y)=\left(\frac{1}{\Delta X}\int_0^{\Delta X}v^2(x,y)dx\right)^{1/2}, \tag{3}$$
$$w_X(z)=\left(\frac{1}{\Delta X}\int_0^{\Delta X}w^2(x,z)dx\right)^{1/2}.$$

It is assumed that $V_X(y)=W_X(y)=0$, which ought to be true for the wake, absent statistical undersampling of structures of coherence length comparable to the window size. The accuracy of the assumption can be verified by measuring the relative magnitudes of mean profile extrema, and here $|U_X|_{\max}/|V_X|_{\max}\geqslant 15$ and $|U_X|_{\max}/|W_X|_{\max}\geqslant 9$. The effect on the turbulence profiles in Figs. 8 and 9 is negligible.

Both $u'_X(y)$ and $u'_X(z)$ can be calculated for horizontal and vertical slices, respectively, and at the centerline,

$$u'_X(z_0)=u'_X(y_0).$$

Subscript-X always refers to a streamwise spatial average, and when applied to a lowercase velocity component, denotes a root-mean-square value. The prime notation refers to unaveraged quantities derived by removing U_X. Hence,

$$\omega'_y=\frac{\partial w}{\partial x}-\frac{\partial u'}{\partial z}. \tag{4}$$

Subscript-0 variables are streamwise-averaged centerline values, and U_0 is the maximum value of either $U_X(y)$ or $U_X(z)$, defining the locations y_0 and z_0, respectively. It should be the case that $U_0(y_0)=U_0(z_0)$ and this can be verified experimentally (Fig. 7).

In both horizontal and vertical slices, a wake region can be defined where $U_X(y)$ or $U_X(z)\geqslant 0.2U_0$. The local wake width and height can be defined this way and are denoted $2L_y$ and $2L_z$, respectively. Averages over the wake are denoted by $\langle\rangle$-brackets. A mean (wake-averaged), turbulent kinetic-energy density is thus

$$\langle e\rangle=\tfrac{1}{2}(\langle u'^2\rangle+\langle v^2\rangle+\langle w^2\rangle). \tag{5}$$

The value at the centerline is

$$e_0=\tfrac{1}{2}(u_0'^2+v_0^2+w_0^2), \tag{6}$$

where u'_0 is available from both horizontal and vertical slices. When the two values differ by less than 10%, they are averaged in Eq. (6), otherwise the time series calculation is terminated.

IV. RESULTS

We begin by showing the vertical and horizontal vorticity fields for this data set. Qualitatively and quantitatively, they agree with those previously shown.[5,13] The focus here is on the best time resolution and on matching time steps in separate experiments with vertical and horizontal slices. Individual vortex patterns are not reproducible from experiment to experiment, but the statistics are.

A. Vorticity fields

Figure 4 shows a time series of the vertical vorticity field, $\omega_z(x,y)$ for $F=4$ and $Re=4860$. Previous experiments[4] show that the flow statistics are quite insensi-

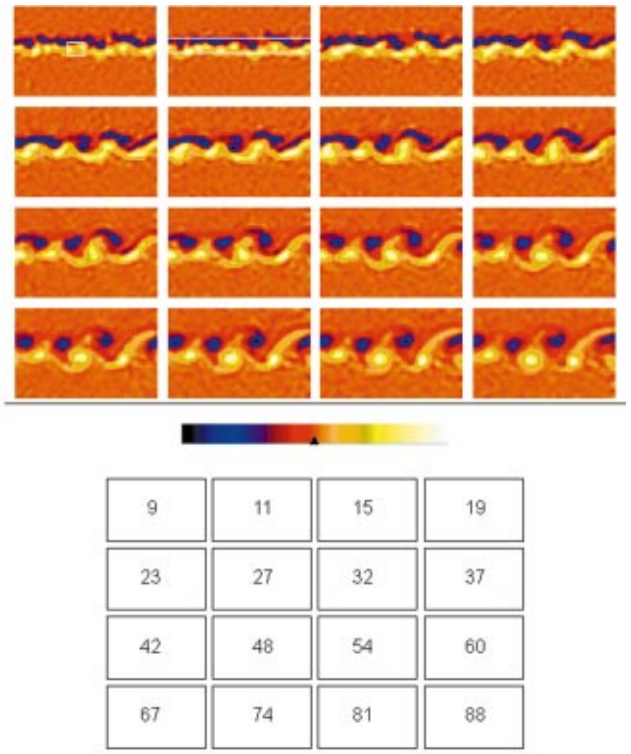

FIG. 4. (Color) Pseudo-color map of $\omega_z(x,y)$ for the time sequence $Nt=\{9-88\}$ (as shown in the box) and $F=4.0$, $Re=4860$. Note how the time interval between successive images increases from $2Nt$ to $7Nt$. The elapsed times correspond $\pm 1Nt$ to the times for the vertical slices in the next figure. The color bar is rescaled about $\omega_z=0$ (shown by the arrow on the color bar) at each timestep. The window size is $\Delta X/D=21.4$ and $\Delta Y/D=13.3$. The sphere travel direction, and hence, mean wake flow, is from right to left.

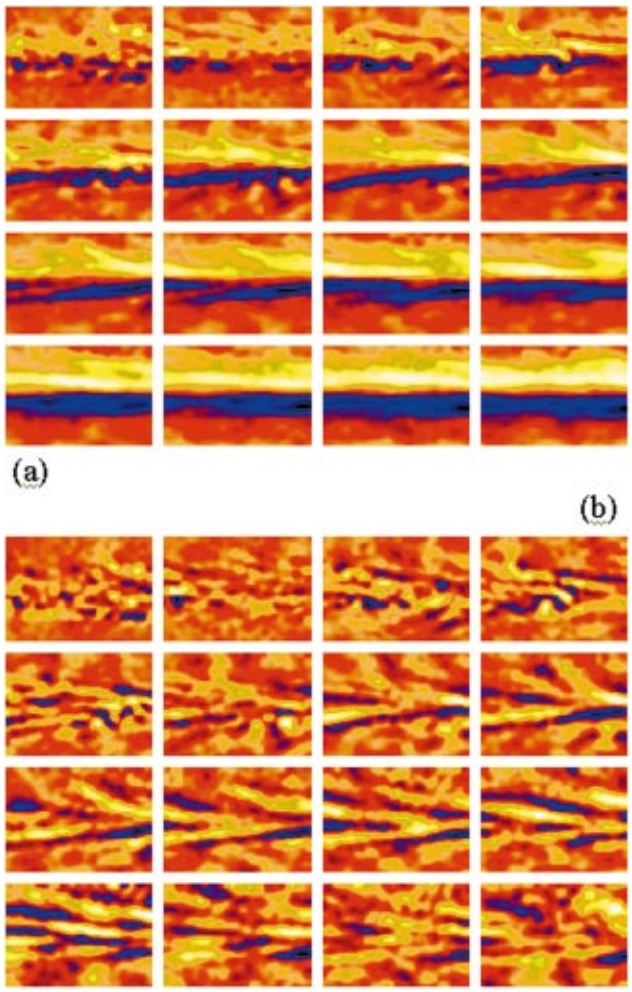

FIG. 5. (Color) $\omega_y(x,z)$ (a) and $\omega_y'(x,z)$ (b) for the same time steps as Fig. 4. $\Delta X/D=2.2$ and $\Delta Y/D=1.61$. The equivalent box size, mapped onto $\{x,y\}$ is shown in the first panel of Fig. 4. Here $F=4$, $Re=7800$, and the mean flow is from left to right.

tive to Re for $4.5\times10^3\leqslant Re\leqslant 8\times10^4$ and also to variations in F for $F\geqslant 4$. Figure 4 can, therefore, be regarded as a canonical example of stratified wakes where the initial values of F and Re are sufficiently high for turbulence to be present over a range of scales. The time period covered, $Nt\in[9,90]$, covers the NEQ régime where the flow is readjusting under the influence of the background stratification. The point at which wake collapse (as traditionally defined by the time when it reaches its first maximum height) occurs ($Nt\approx 2$) has long since passed, and so the effects of the restoring buoyancy forces are being felt, at least at the larger scales, at all times in the figure. The most notable feature is the relatively orderly arrangement of coherent structures which have already formed in the top left panel, and which grow in size and decrease in number by merging of pairs or triplets of like-signed vortices. One pairing event can be followed by tracking the contents of the outlined box in the first frame. Most of the pairing interactions are complete by the end of the third row ($Nt\approx 60$), after which further interactions are infrequent. Between the first frame at $Nt=9$ and the end of the third row at $Nt=60$, the vortex structures are elongated in the streamwise direction, apparently due to both incipient merging interactions and straining by the mean wake profile.

Note that the equivalent averaging time $\Delta Nt=\frac{1}{2}\Delta x/D\approx 10$ is not small compared to the frame interval in Fig. 4. Thus the wake evolution of the right edge of a single frame has occurred over a longer interval than at the left of the frame, and this time usually exceeds the frame-to-frame interval. Data from neighboring time steps are, therefore, not independent, and quantities derived from this sampling interval may be regarded as smoothed over a window that includes up to three time steps.

The horizontal vorticity, $\omega_y(x,z)$ is shown for the same equivalent time series in Fig. 5(a), and with the mean wake profile removed $[\omega_y'(x,z)]$ in Fig. 5(b). The difference between the two reflects the dominating influence of the mean wake shear on the colormap, and presumably on the dynamics too. Note carefully that the field of view is about 1/10th the size of the previous figure. Initially, there are cross sections through many small-scale structures with a degree of apparent randomness that contrasts sharply with the pattern already visible in the horizontal plane (same panels, previous figure). The top two rows show the development of structures that are elongated in the x direction, and tilted so they form a v-shape pointing in the direction of motion. It is well known that for $F\geqslant 4$, the evolving turbulent wake can generate internal waves in a stratified fluid[14–16] in this interval, and the tilted structures often appear to have a periodic, spatially extended pattern. It is not so straightforward to distin-

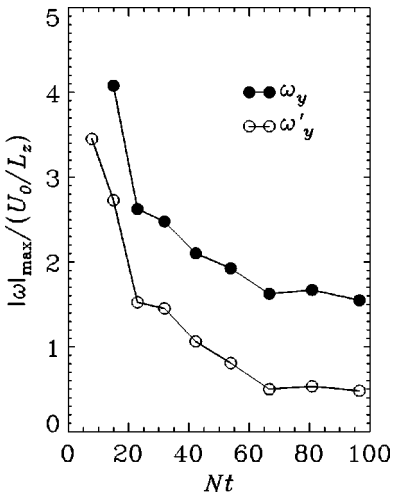

FIG. 6. The evolution of maximum absolute values of $\omega_y(x,z)$ and $\omega_y'(x,z)$, rescaled by local values of U_0/L_z.

guish wave and vortex modes at early times, but two characteristics are clear in the $\omega_y'(x,z)$ field of Fig. 5(b): (i) There are spatially extended regions of alternating-sign, horizontal vorticity, with similar dominant lengthscale; (ii) the disturbance does not remain localized in the wake center, but has spread to the far field. It seems reasonable to assume that periodic, propagating components can be described as waves. Their presence will also be apparent in the streamwise-averaged turbulence profiles.

Initially, peak values of ω_y are three to four times the mean shear, defined by the wake half-height and local defect magnitude (Fig. 6). The upper and lower wake shear layers eventually account for most of the coherent vorticity, but not all of it, as shown by the remaining $|\omega_y'|_{max} \simeq 0.5(U_0/L_z)$ and the nonrandom patterns in Fig. 5(b). The persistent difference of approximately $1(U_0/L_z)$ between the top and bottom curves shows that at $F=4$, the vertical wake structure is well approximated as a single dominant wake profile, with single vertical scale L_z, on top of which ride a number of weaker disturbance profiles or structures. Further discussion on this and related points can be found in Ref. 13.

B. Mean flow and turbulence profiles

Figure 7 compares the mean streamwise velocity profiles, $U_X(y)$ and $U_X(z)$ for horizontal and vertical cuts through the wake centerline. At the centerline, one can verify that $U_X(y_0)=U_X(z_0)=U_0$. When there is a difference, $U_X(z_0)$ tends to fall beneath $U_X(y_0)$ because horizontal profiles are taken from isopycnal measurements, while vertical plane measurements come from a fixed planar sheet. Any meandering or undulating of the wake away from the geometric centerline will (a) be reduced in the vertical due to the stratification, and (b) will give a larger velocity when projected from an isopycnal rather than an oblique, off-center cut.

The scales in y and z differ by a factor of 4 and so the coincidence of the filled circles and squares in the first panel indicates a mean wake aspect ratio of about 1:4 or 0.25. The aspect ratio decreases further with time as the circles move

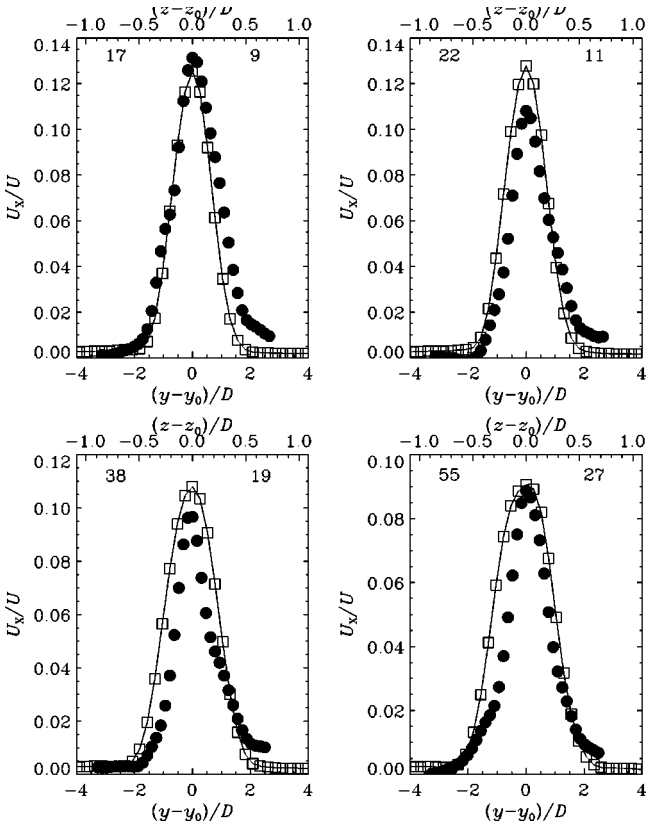

FIG. 7. Mean horizontal $[U_X(y), \square]$, and vertical $[U_X(z), \bullet]$ wake profiles normalized by the sphere diameter, D, and velocity, U. x/D and Nt are shown in the top left and top right of each panel. The scales in y (lower) and z (upper) are not equal.

inside the horizontal profile. It is these mean profiles that are removed from the $\{u,v\}(x,y)$ and $\{u,w\}(x,z)$ fields to produce the fluctuating velocity profiles.

The turbulence profiles of $u_X'(z)$ and $w_X(z)$ (Fig. 8) are slightly, but importantly different at the first measurable time step, $Nt=3$. The centerline (z_0) values of w_X are lower than u_X' (note the different vertical scales) and while the peak location in z is the same (inside one sphere radius), the tails of $w_X(z)$ fall more slowly with increasing vertical distance from the centerline. As time goes by, the peaks in $w_X(z)$ move outward toward the wake periphery, and the magnitude of w_X significantly exceeds u_X' there. The largest fluctuations in u_X' are confined to a narrow region about one sphere radius in vertical extent, where they are significantly larger than w_X. A strong anisotropy in the turbulence profiles has developed, characterized by the association of the largest vertical velocity fluctuations with wave modes that move away from the wake centerline at a rate that is faster than the mean growth rate of the wake profile itself (see previous figure), and the confinement of the horizontal fluctuations to a very narrow layer in the vertical. The process continues in the lower panels of Fig. 8, as the peaks in w_X move outwards, while the u_X' values become more evenly distributed across the wake center.

The results can be compared with literature data on wakes in homogeneous fluids at similar Re. Bevilaqua and Lykoudis[17] found peak values of $u'/U \simeq 0.03$ in the sphere

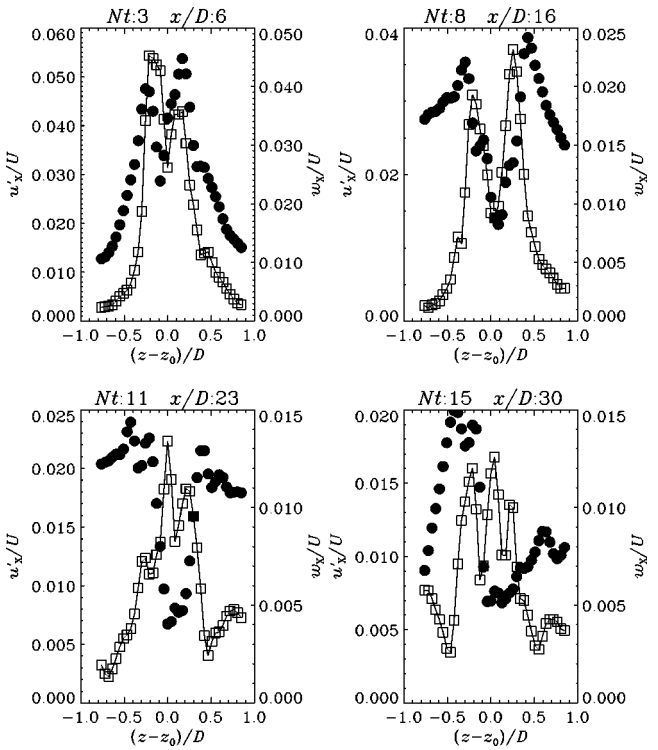

FIG. 8. The evolution of streamwise averaged, vertical profiles of fluctuating horizontal, (u'_X, □) and vertical (w_X, ●) velocities for four $\{Nt, x/D\}$ values. The line connecting the u'_X values is for clarification only. The two ordinate scales vary with time and with respect to each other.

wake, and 0.055 in the wake of a disk with the same drag, at $x/D=6$ and for $Re=10^4$. Note that u' is a temporally averaged quantity, as is more usually the case in turbulence studies. In Fig. 8(a), maximum values of u'_X/U are approximately 0.055, while $(w_X/U)_{\max}\simeq 0.045$. The differing averaging techniques and Reynolds numbers make direct comparison hazardous, but the fluctuation magnitudes appear to be similar.

Uberoi and Freymuth[18] report details primarily in the self-similar region at higher x/D for a sphere at Re$=8.6\times10^3$. At $x/D=20$, $u'/U_0\simeq 0.14$ from their Fig. 2. At $x/D=20$, $u'_X/U\simeq 0.02$ from Fig. 8, and $U_0/U\simeq 0.12$ from Fig. 7, so the equivalent measure, $u'_X/U_0\simeq 0.17$. However, they note that until self-similarity is reached, u'/U_0 increases with x/D, so that at $x/D=30$, $u'/U_0\simeq 0.18$. Again, from data in Figs. 7 and 8, the stratified wakes give $u'_X/U_0\simeq 0.14$ for $x/D=30$. The normalized turbulence intensities in the stratified wake are falling, not rising.

The stratified wake has two competing tendencies. In the early wake, $x/D\leqslant 20$, the peak turbulence intensities are higher than the nonstratified equivalent. This is not so surprising since classically u' scales as U_0 does, and it has previously been established[4,8] that U_0 decays much more slowly with x/D in stratified wakes. At the same time, the opposing tendency is for buoyancy forces to constrain the motion and damp out fluctuating components, at least in z. During NEQ, the $F_{\text{loc}}=1$ condition occurs at the wake edge allowing kinetic energy associated with w to excite internal waves, which then propagate away from the wake (Fig. 8). Simultaneously, it is conjectured that some potential energy is returned to kinetic energy that feeds both U_X and u'_X: The wake-averaged redirection potential and kinetic energy to the horizontal component of velocity, u_H can be at the expense of both w and potential energy.

The fluctuating profiles of u'_X and w_X from vertical slices are shown in Fig. 8 (left and right columns). In many respects, as u'_X and w_X are parallel to the mean wake forcing, and to the gravitational restoring force, they contain much of the signature of the developing wake anisotropy. However, a composite picture of all three components drawn from appropriately matched horizontal and vertical plane data shows further unique characteristics. Figure 9 shows $u'_X(y,z)$, $v_X(y)$, and $w_X(z)$ for $x/D=\{17,\ 22,\ 54\}$. Note that the two profiles of u'_X should coincide at the centerline, (y_0,z_0), and they do.

The different shape of the u'_X profiles in y and z is immediately striking. The magnitude of $u'_X(z,z\neq z_0)$ is significantly higher than its counterpart in y in the first row ($x/D=17$), and the y-profile does not show the two sharp off-centerline peaks. Recall that in Fig. 8 the shape and magnitude of u'_X and w_X were quite closely matched at early times. The top left panel of Fig. 9 corresponds in Nt, x/D to the mean profiles in the top left panel of Fig. 7, and it appears that the maximum $u'_X(z)$ fluctuations occur in the mean shear layers above and beneath the already nonround ($L_z<L_y$) wake. Qualitatively similar $w_X(z)$ peaks (top right) are already moving out from the wake centerline, as previously noted in Fig. 8, and continue to do so (right column of Fig. 9). Observe carefully that $u'_X(y)$ also has a double-peaked shape, maximum fluctuations occurring also at the shear layers in the horizontal profile (again, see Fig. 7).

With increasing x/D or Nt (i.e., moving down to rows 2 and 3 in Fig. 9), the u'_X fluctuations in y and z reach similar magnitudes but those in z are much more confined close to the centerline, z_0. At the same time, the $v_X(y)$ profiles show a completely different shape with a strong peak at the centerline, which is maintained over this time sequence. The smaller peaks of about half the amplitude on either shoulder occur not at the location of maximum mean $\partial U_X/\partial y$ (see Fig. 7), but at the very outer limit of the wake at $y/D\approx 2$. Horizontal lines at $y/D=\pm 2$ have been superimposed on the $\omega_z(x,y)$ plot of Fig. 4 in frame #2, which is the same data upon which the center panel of $u_X(y)$ in Fig. 9 is based. The lines trace the outer edge of the early wake vortex structures, when the basic wake shape is still quite straight. Since the $v_X(y)$ secondary peaks appear closer to the edge of the vortices, rather than directly through their center, they may be associated with internal wave generation at the interface between the wake vortices and the relatively undisturbed ambient stratification.

The most prominent characteristic of the $v_X(y)$ profiles is the strong peak at the centerline, whose magnitude exceeds that of the peaks in $u'_X(y)$ by $x/D=54$. The profile shape is very different from the u'_X and w_X components, and very different from the unstratified equivalent (refs. cit.), but then so is the wake vorticity distribution also. The last row in Fig. 9 corresponds to frame #6 in the time series of Figs. 4

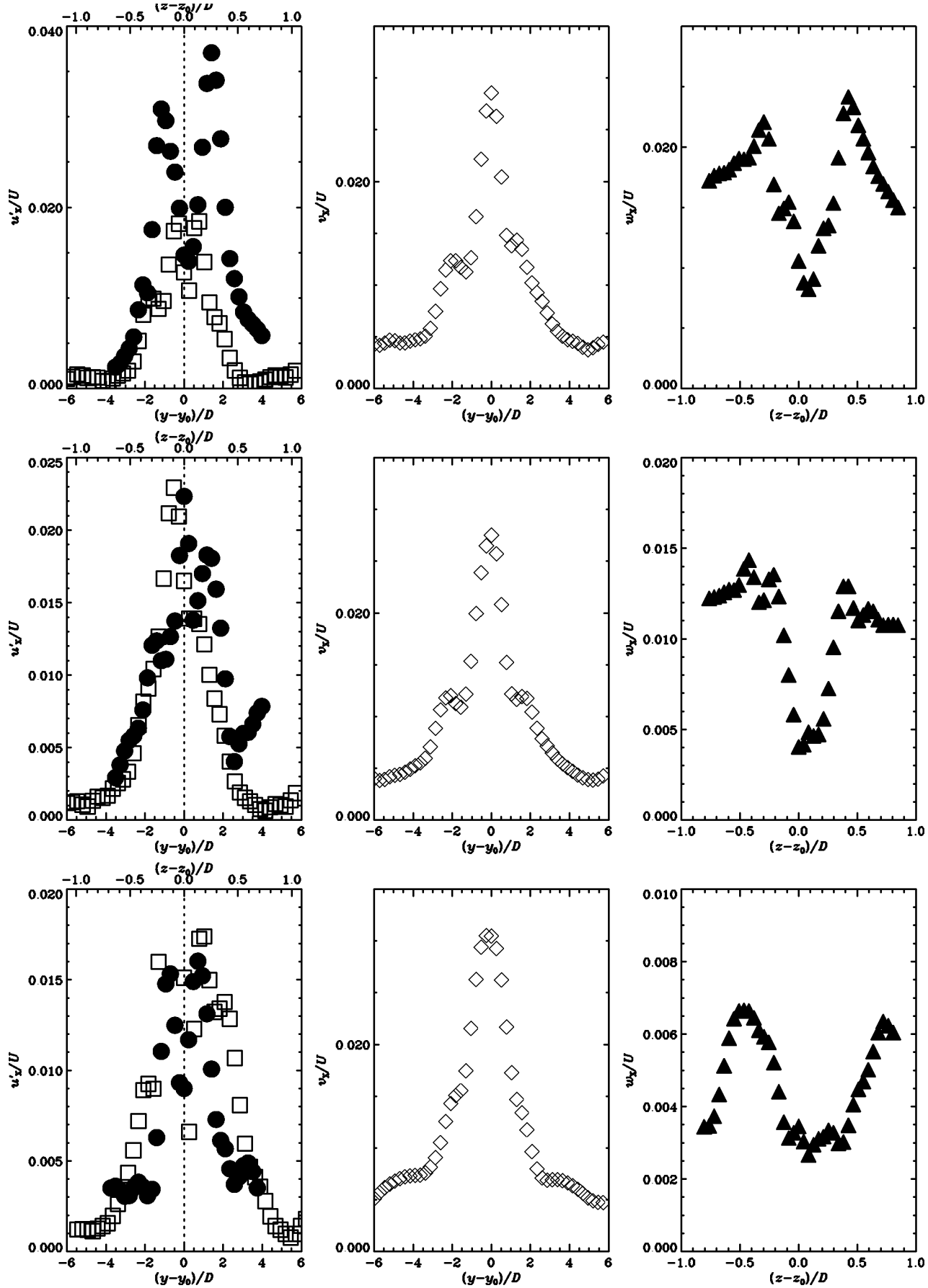

FIG. 9. Horizontal (open symbols) and vertical (filled) fluctuating velocity profiles for $Nt=\{9,11,27\}$, translating to 1.4, 1.75, and 4.3 buoyancy periods, respectively, from top to bottom row. In the left column, u'_X is plotted as a function of $(y-y_0)$ (bottom axis) and w_X is plotted against $(z-z_0)$ (top axis).

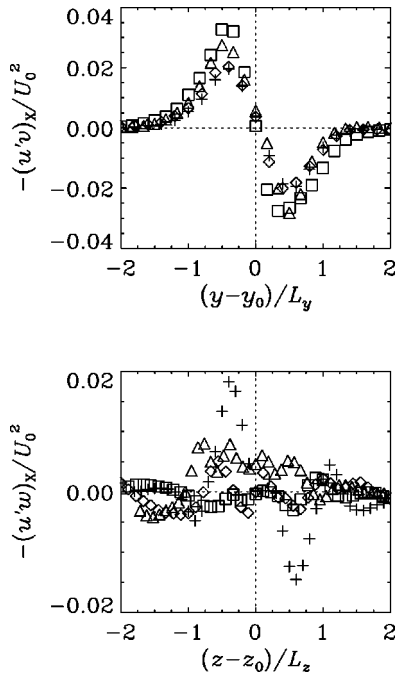

FIG. 10. Streamwise-averaged Reynolds stress terms, $u'v$ and $u'w$, normalized by local maximum wake defect velocity, U_0 at $x/D=\{17, 22, 30, 38\}$ for symbols $\{+,\diamond,\triangle,\square\}$. y and z axes are normalized by the local wake half-width, L_y and half-height, L_z, respectively. (L_y grows from $\approx$4.6–5.9 cm while L_z remains roughly constant at $\approx$1.6 cm during this time).

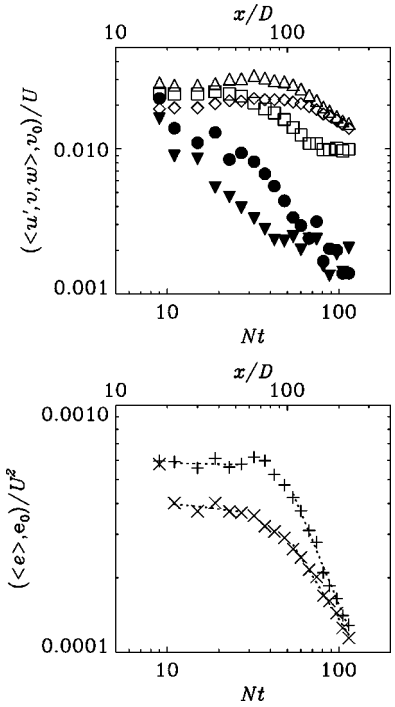

FIG. 11. (a) Wake-averaged fluctuating velocities from horizontal (open symbols) and vertical (filled) profiles. $\langle u'\rangle$ and $\langle v\rangle$ are shown by $\square$ and $\diamond$. $\langle u'\rangle$ and $\langle w\rangle$ from vertical profiles are shown by $\bullet$ and filled $\diamond$. The $\triangle$'s are for v_0, averaged along the centerline only. (b) Turbulent kinetic energy averaged over the whole wake, $\langle e\rangle,\times$, and along the centerline only, e_0, $+$.

and 5. Other than the rather regular spacing of the rather coherent structures, the other notable (related) feature of the wake is the undulation at the wake centerline. This is the main contributor to the high $v_X(y_0)$, and unstratified wakes do not have this feature.

The Reynolds stress terms $(u'v)_X$ and $(u'w)_X$ (spatial equivalents of the usual $\overline{uv}$ and $\overline{uw}$) can be calculated in horizontal and vertical profiles, respectively, and are shown in Fig. 10 for four different values of x/D. The abscissa is normalized by the local wake length scale, L_y or L_z, and the Reynolds stresses themselves are normalized by the local U_0^2. The $(u'v)_X$ component has a similar distribution to that expected in an unstratified wake, but the curves do not collapse, showing that the fluctuating velocity profiles have not yet, or have only just, reached a self-similar state by $x/D=38$. The vertical profiles are extremely different. At $x/D=17$, $(u'w)_X$ is similar in shape and magnitude to $(u'v)_X$, but reverses sign at about L_z from the centerline, z_0. At $x/D=22$ (diamonds), the maximum magnitude is less than one-third of the previous curve, and the shape is quite irregular, but still changes sign at the wake edge. This pattern continues until by $x/D=38$ (squares) little structure can be discerned and the amplitude is very small. The measurement cannot be extended to later times because by now the streamwise coherence length of structures in the vertical slices has become comparable to the observation box size and statistics do not converge.

C. Turbulent kinetic-energy decay

The downstream decay of all measurable fluctuating velocity components is shown in Fig. 11(a). The decay of $\langle u'\rangle$ and $\langle w\rangle$, averaged over the wake in the vertical direction (filled circles and diamonds), is much faster than the equivalent measures of $\langle u'\rangle$ and $\langle v\rangle$ on a horizontal centerplane (open squares and diamonds). The rapid decay of $\langle u'\rangle$ and $\langle w\rangle$ is particularly notable between the first two time steps, and is due to the previously noted departure of internal wave energy from the wake domain. The open triangles also show the result for v_0. Both $\langle v\rangle$ and v_0 decay more slowly than the other quantities, reflecting the persistence of the strong peak at the centerline seen in Fig. 10.

The results can be added, as in Eqs. (5) and (6), to give measures of the turbulent kinetic-energy decay. $\langle e\rangle$ is an averaged energy density from both horizontal and vertical centerplanes. e_0 is the average energy density at the centerline only. They are plotted as $\times$ and $+$ symbols in Fig. 11(b). Both $\langle e\rangle$ and e_0 begin at the same value, but the wake-averaged $\langle e\rangle$ drops immediately as the contribution from internal wave motions decreases when the waves propagate away from the wake. This contribution is not very important at the centerline itself, and e_0 remains almost unchanged up to $Nt\approx30$. Following its initial drop, $\langle e\rangle$ also changes little during the same time period. After $Nt=30$, e_0 decays more rapidly than $\langle e\rangle$, a trend that is fuelled by the eventual decline in v_0. Nominal decay rates with Nt or x/D are -1.1 for $\langle e\rangle$, and -1.7 for e_0. They bracket previous horizontal plane measurements[4] that show a $-4/3$ decay for wake-averaged energy in the late wake ($Nt>50$).

Note that Fig. 11(b) cannot claim to be a complete energy budget for the system because all measured components

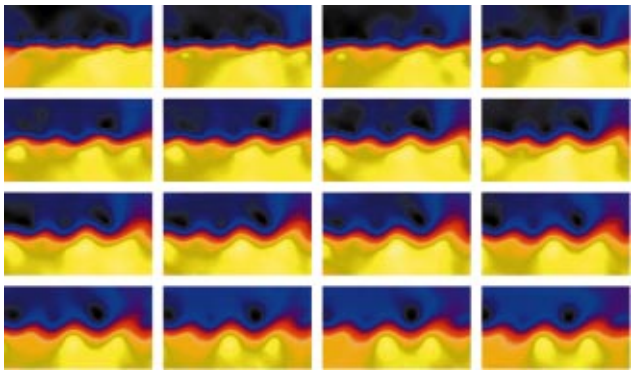

FIG. 12. (Color) Streamfunction, $\psi(x,y,Nt)$ for the same data as Fig. 4. The wake is moving past the stationary laboratory frame of reference.

come from either horizontal or vertical centerplanes. Most internal wave energy propagates at some intermediate angle, typically around 45 deg, and will not be sampled this way, as implicit in the interpretation of Fig. 11.

The observed decay of the turbulent fluctuations and the profile shapes suggest the following physical picture of the wake evolution.

D. Wake instability?

1. Observations from data

The principal cause of the high values of v_X, and particularly v_0, documented in the previous section is illustrated in Fig. 12, which is a plot of the streamfunction, calculated from

$$\psi_P = \psi_0 + \int_0^P (u\,dy - v\,dx). \tag{7}$$

At any point, P, in the rectangular grid, the integral along two alternative paths around each grid cell are averaged, and the effect of cumulative errors together with uncertainty about assumptions concerning the original starting value P_0 (the obvious choice of $u=v=0$ in the far field is not correct because internal waves have spread there even at early times) are minimized by averaging the result from a number of different starting locations.

The most prominent feature of Fig. 12 is the regular sinuous oscillation at the wake centerline, whose amplitude grows significantly up to the end of the second row ($Nt=37$). Velocity vectors that were initially quite straight (frame #1) in the early wake end up being significantly deflected, particularly at the centerline. To understand why v_X would reflect this more strongly than u'_X, consider an initially horizontal vector at the centerline with $u=U_0$, $v=0$, and then imagine a perturbation that deflects it through a small angle, θ. Now $u=U_0\cos\theta$ and $v=U_0\sin\theta$, and

$$\frac{\partial u}{\partial \theta} \sim u' \sim -\sin\theta,$$

$$\frac{\partial v}{\partial \theta} \sim v' \sim \cos\theta.$$

Clearly $|v'|>|u'|$ when $\theta<\pi/4$, thus $v'=v$ dominates the turbulent fluctuations close to the centerline. A similar argument applies of course to $w=w'$, but w can enter wave modes that leave the wake, and vertical fluctuations with time scales very different from N^{-1} are eventually extinguished by the constraining influence of buoyancy forces.

The argument is simple and appears successful, but it has a built-in asymmetry because it assumes an initial perturbation of a form that deflects velocity vectors laterally. Figure 12 certainly looks like an instability that has this effect, as a straight wake rumples up into a quite regular sinuous form, and it is worth examining the extent to which such a wake instability can account for the origin of the late-wake ''pancake'' eddies themselves.

Despite the relatively large amount of data that has been accumulated for stratified wakes, there is considerable uncertainty about the physical mechanism for the formation of the late wake eddies. The question can be simplified into deciding whether they originate as a remnant of an instability of vortex shedding at the body surface, or whether they come from a wake instability, without special reference to the initial conditions. Put in these terms, the solution has evident consequences for the generality of solutions for particular body shapes. The following arguments suggest that the original simplification of the question might be difficult to maintain.

The wavelength of the wavy disturbance of the streamlines in Fig. 12 does not change greatly over the time it is observable (from $Nt=11$ in frame #2 to $Nt=88$ at the end of the time series), with $n_\lambda=3.5-4$ wavelengths per observation box. The observation box has streamwise length, $\Delta X/D=21.4$ and so defining a Strouhal number, $St=n_\lambda/(\Delta X/D)$, St varies between 0.187 and 0.16. St for the predicted spiral mode instability is 0.175. The agreement is either coincidental, or a wake instability is forced by the wavelength of the pre-existing spiral mode, or there is no additional intrinsic wake instability, and the collapsed remnant of the spiral mode accounts for the periodic signature.

It is instructive to look at the arrangement of vortices in Fig. 4 together with Fig. 12. Initially, the number of vortices does not have a simple correspondence with the wavy wake. In the first two rows, discrete vortex patches can be observed being clustered together in two's or three's. Members of a cluster merge so that by the bottom row ($Nt>60$), the vortex number and spacing does correspond with the wavy instability. Furthermore, a rough count at the first timestep, shows at least 10 vortices of each sign over ΔX, corresponding to $St=0.47$. This cannot have come from a spiral mode.

2. Comparison with previous studies

The origin of characteristic frequencies in the near wake of towed spheres in a stratified fluid was considered in detail by Chomaz *et al.*,[19] who showed that at sufficiently high values of F and Re (such as the case in this paper), the near wake contains two frequencies: One associated with a Kelvin–Helmholtz (KH) instability of the detached free shear layer, and one longer wavelength associated with a spiral shedding mode. Their results thus confirmed the re-

sults of Kim and Durbin[20] for the homogeneous wake. St for the KH mode scales as $\sim Re^{1/2}$ (as does the boundary-layer thickness on the sphere, and hence the free shear-layer thickness in the near wake), and has a value of approximately 1.4 at $Re=5\times10^3$. Between 1 and 2 pairings could account for the observed value of $St=0.47$ at $x/D=17$. If an initial eddy turnover time scales as D/U, then 17 turnover times have elapsed before frame #1 in Figs. 4, 5, and 12.

A third wake instability mode was identified by Chomaz *et al.*,[19,21] who observed vertical wake oscillations in a near wake transition régime in the range $0.9\leqslant F\leqslant 4.5$. However, at $F=4$ the instability amplitude can be inferred from their data to have fallen to less than 0.1 D, and St is at the same time indistinguishable from that of the spiral mode. Although such a near-wake instability could provide a mechanism for early preferred grouping of coherent structures at moderate F, St values of ≈ 0.5 seen in Fig. 4 for $F=4$ are not explained.

In a numerical and experimental study of the instability of a laminar, flat-plate Gaussian wake profile, Sato and Kuriki[22] found maximum growth rates to small disturbances around a dimensionless frequency, $2\pi fb/U_0=0.5$ in the high Reynolds number limit and ~ 0.6 in experiments where $Re=U_0b/\nu=500-1000$. The length scale, b, is the wake half-width. Since the initial conditions here are much more complicated and irregular (moving boundary-layer separation points, free shear flow instabilities with vortex roll-up, fully three-dimensional flow), it is not so clear how to make a direct comparison. Assigning $b=3.0$ cm, based on the mean profile geometry at the earliest available data when $x/D=17$, the Sato and Kuriki (SK) frequency is related to the Strouhal number as

$$\hat{f}_{\mathrm{SK}}=2\pi \mathrm{St}.\frac{b}{D},$$

and when $St=0.175$, $\hat{f}_{\mathrm{SK}}=0.87$, which lies far from the 0.5–0.6 range. If $b=D/2$ is set as an initial length scale, then $\hat{f}_{\mathrm{SK}}=\pi St=0.55$ for the long wavelength instability observed here (Fig. 11). However, the short wavelengths observed at the earliest time steps (top of Fig. 4) still yield $\hat{f}_{\mathrm{SK}}=1.48$ and so cannot be explained this way.

The experimental evidence alone does not preclude further alternative long-wave forcing mechanisms of the initially straight wake. For example, observed values of the Strouhal number are very close to the 0.21 seen in the two-dimensional von Kármán street, and may simply reflect a temporarily stable and preferred spacing before further pairing reduces St even further. Ultimately, the preferred explanation is the simplest one which can account for the observations.

3. The most likely cause

The combination of KH and spiral mode instabilities alone can account for the observed wavelengths in the wake. However, if the question is: ''What causes the late-wake eddies?,'' Figs. 4 and 12 show that a combination of instabilities and pairing–merging mechanisms is responsible. Now that numerical experiments[10,11] of sufficient resolution are emerging to investigate aspects of this flow, a combination of numerical and experimental approaches might be able to answer some different, but equally interesting questions, such as ''Under what circumstances, and how, is information concerning the body geometry preserved in the wake?'' and ''What are the special characteristics of stratified wakes that allow the undisrupted evolution of the initial instability modes?''

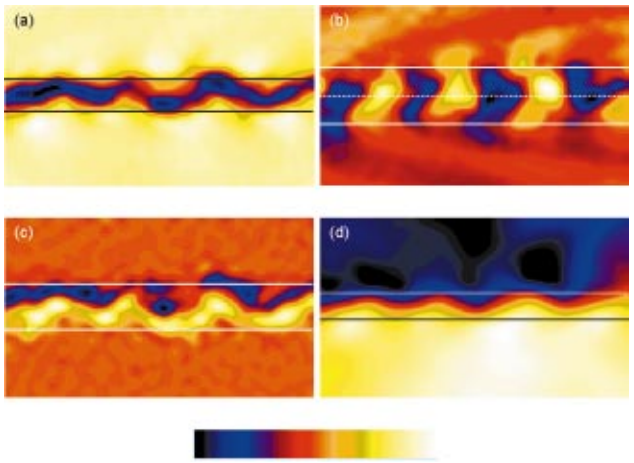

FIG. 13. (Color) Field variables and their relation to wake-profile averaged quantities. (a) $u(x,y)$, (b) $v(x,y)$, (c) $\omega_z(x,y)$, and (d) $\psi(x,y)$ for $Nt=19$, $x/D=39$. In all cases $\Delta X/D=21.4$ and $\Delta Y/D=12.2$. The standard color bar is scaled over $\pm|f|_{\max}$, where f is the field variable above, and symmetrically around $f=0$, except for u. In the corresponding panel, horizontal lines show: (a) point of $(u'_X)_{\max}$, $y/D=\pm1.15$; (b) points of $(v_X)_{\max}$ which are at the centerline, y_0 (dotted line), and at $y/D=\pm2$; (c) local mean wake width, $2L_y$, and (d) point of $|(u'v)_X|_{\max}$ at $L_y/2$.

E. Summary and conclusions

The $F=4$, $Re\simeq5\times10^3$ case is a convenient point for a detailed investigation of initially turbulent wakes that decay in the presence of a stable background density gradient. Turbulence is present over some minimum range of scales and power law scaling of wake-averaged quantities seems to be applicable over 2 orders of magnitude extension in F and Re. At the earliest times accessible to experiment, $Nt=9$, $x/D=17$, the wake height is already much smaller than the wake width, so the larger scales are always strongly anisotropic. The turbulence profiles begin with similar magnitudes in all three directions, but the vertical fluctuations, w_X, close to the wake centerline decay more rapidly than the horizontal fluctuations, u'_X, and the peak values of w_X become associated with internal wave modes, which move away from the wake center. $v_X(y)$ and $w_X(z)$ profile shapes are quite different from $u'_X(y)$ and from literature results for turbulent wakes at similar Re in homogeneous fluids. The profile shapes can be related to the known vorticity distributions, and a physical interpretation of the unique characteristics of the turbulence profiles can be made. Figure 13 illustrates and summarizes some of the main points.

The u velocity component [Fig. 13(a)] is dominated by the mean wake flow and is closely confined to the centerplane. The rather slow growth of the wake in y is one of its distinguishing characteristics, and the average maximum

fluctuation magnitudes occur close to an envelope that encloses the undulating wake defect. By contrast, the peak v_x values occur right at the centerline [dotted line in Fig. 13(b)], with intermediate maxima at the border of the central islands of $v(x,y)$. The v-component also has nonzero, nonrandom values in the far field, caused by lee waves from the sphere body. These are responsible for the nonzero tails in $v_X(y)$ in Fig. 9. As noted on previous occasions the coherent structures in $\omega_z(x,y)$ remain packed close to the centerline, and the lines of $\pm L_y$ in Fig. 13(c) enclose almost all the vertical vorticity. The vortex patches themselves are shown undergoing pairing and triplet interactions, which will clump the remaining patches into a wake spacing that closely matches that predicted by a spiral mode instability. The collapsed remnant of the spiral mode may be sufficient to force a wake instability, a suspicion that is encouraged by the remarkably regular undulations that grow in $\psi(x,y)$ close to $y=y_0$. A lateral deflection of the streamwise velocity vector will generate high values of v_X, concentrated at y_0, as measured. The peak Reynolds stresses [horizontal lines in Fig. 13(c)] occur exactly at the boundary of the closely spaced streamlines (large $\partial u/\partial y$).

Although the wake undulations look very much like a profile instability, such an explanation is not required to explain the observed wavelengths in the wake, which can plausibly have been generated by the known Kelvin–Helmholtz and spiral mode instabilities alone. The most parsimonious explanation therefore does not (yet) require a new self-induced profile instability.

The NEQ phase of evolution of the stratified wake is where it distinguishes itself from its counterpart in a homogeneous fluid. The data shown here encompass the approximate range $Nt \in [10,100]$, when strongly three-dimensional flow is converted to almost entirely two-dimensional motion. The larger length scales of order D first are affected by the background density gradient, before $Nt=10$. At $Nt=10$, the turbulence profiles themselves begin to be affected in magnitude. Strong variation in the shape, and differences from the homogeneous fluid equivalent are visible already, and they continue to evolve in ways that reflect the emission and propagation of internal waves into the far field, the selective damping of w in the wake itself, and the slow initial decay of turbulent kinetic energy in the wake.

The relatively high kinetic-energy density in the wake can be seen as an inevitable consequence of the very slow initial vertical growth rates, without any (perhaps expected) concomitant increase in horizontal growth rates beyond the homogeneous case. In a well-controlled experiment, the tightly clustered wake vortices maintain the compact geometry of the induced flow between them. The vortices do not form *independent* dipoles, tripoles etc., but even when merging, remain close to the wake centerline. This fact argues for a regular pattern of interlocking of vortex lines[4] along the stratified wake that does not occur in a homogeneous fluid, and further work is required to discover the nature and evolution of this vortex geometry.

ACKNOWLEDGMENTS

Jun Chen worked very hard on collecting the data upon which this manuscript is based, and Professor F. K. Browand provided valuable advice and discussion. The support of ONR Grant No. N00014-96-1-0001 under Dr. L. P. Purtell is most gratefully acknowledged.

[1] J. T. Lin and Y. H. Pao, "Wakes in stratified fluids: A review," Annu. Rev. Fluid Mech. **11**, 317 (1979).
[2] E. J. Hopfinger, "Turbulence in stratified fluids: A review," J. Geophys. Res. **92**, 5287 (1987).
[3] J. J. Riley and M.-P. Lelong, "Fluid motions in the presence of strong stable stratification," Annu. Rev. Fluid Mech. **32**, 613 (2000).
[4] G. R. Spedding, F. K. Browand, and A. M. Fincham, "Turbulence, similarity scaling and vortex geometry in the wake of a sphere in a stably-stratified fluid," J. Fluid Mech. **314**, 53 (1996).
[5] G. R. Spedding, "The evolution of initially-turbulent bluff-body wakes at high internal Froude number," J. Fluid Mech. **337**, 283 (1997).
[6] J. J. Riley, R. W. Metcalfe, and M. A. Weissman, "Direct numerical simulations of homogeneous turbulence in density stratified fluids," in *Nonlinear Properties of Internal Waves*, AIP, edited by B. J. West (AIP, New York, 1981), pp. 79–112.
[7] J.-M. Chomaz, P. Bonneton, A. Butet, and E. J. Hopfinger, "Vertical diffusion in the far wake of a sphere moving in a stratified fluid," Phys. Fluids A **5**, 2799 (1993).
[8] G. R. Spedding, F. K. Browand, and A. M. Fincham, "The long-time evolution of the initially-turbulent wake of a sphere in a stable stratification," Dyn. Atmos. Oceans **23**, 171 (1996).
[9] G. R. Spedding, "Vortex wakes in stably-stratified fluids," in *Simulation and Identification of Organized Structures in Flows, Proceedings of the IUTAM Symposium*, edited by J. N. Sorensen, E. J. Hopfinger, and N. Aubry (Kluwer, Dordrecht, The Netherlands, 1999), pp. 163–179.
[10] D. G. Dommermuth, J. W. Rottman, G. E. Innis, and E. A. Novikov, "Numerical simulation of the wake of a towed sphere in a weakly stratified fluid," in *Stratified Flows I, Proceedings of the 5th Internatioanl Symposium on Stratified Flows*, edited by G. A. Lawrence, R. Pieters, and N. Yonemitsu (UBC, Vancouver, Canada, 2000), pp. 37–42.
[11] M. J. Gourlay, S. C. Arendt, D. C. Fritts, and J. Werne, "Numerical modeling of turbulent non-zero momentum late wakes in density stratified fluids," in *Stratified Flows I, Proceedings of the 5th International Symposium on Stratified Flows*, edited by G. A. Lawrence, R. Pieters, and N. Yonemitsu (UBC, Vancouver, Canada, 2000), pp. 67–72.
[12] A. M. Fincham and G. R. Spedding, "Low-cost, high-resolution DPIV for turbulent flows," Exp. Fluids **23**, 449 (1997).
[13] G. R. Spedding, "Vertical structure in stratified wakes with high initial Froude number," J. Fluid Mech. (to be published).
[14] H. E. Gilreath and A. Brandt, "Experiments on the generation of internal waves in a stratified fluid," AIAA J. **23**, 693 (1985).
[15] P. Bonneton, J.-M. Chomaz, and E. J. Hopfinger, "Internal waves produced by the turbulent wake of a sphere moving horizontally in a stratified fluid," J. Fluid Mech. **254**, 23 (1993).
[16] G. R. Spedding, F. K. Browand, R. Bell, and J. Chen, "Internal waves from intermediate, or late-wake vortices," in *Stratified Flows I, Proceedings of the 5th International Symposium on Stratified Flows*, edited by G. A. Lawrence, R. Pieters, and N. Yonemitsu (UBC, Vancouver, Canada, 2000), pp. 113–118.
[17] P. M. Bevilaqua and P. S. Lykoudis, "Turbulence memory in self-preserving wakes," J. Fluid Mech. **89**, 589 (1978).
[18] M. S. Uberoi and P. Freymuth, "Turbulent energy balance and spectra of the axisymmetric wake," Phys. Fluids **13**, 2205 (1970).
[19] J.-M. Chomaz, P. Bonneton, and E. J. Hopfinger, "The structure of the near wake of a sphere moving horizontally in a stratified fluid," J. Fluid Mech. **254**, 1 (1993).
[20] H. J. Kim and P. A. Durbin, "Observations of the frequencies in a sphere wake and of drag increase by acoustic excitation," Phys. Fluids **31**, 3260 (1988).
[21] P. Bonneton, J.-M. Chomaz, E. J. Hopfinger, and M. Perrier, "The structure of the turbulent wake and the random wave field generated by a moving sphere in a stratified fluid," Dyn. Atmos. Oceans **23**, 299 (1996).
[22] H. Sato and K. Kuriki, "The mechanism of transition in the wake of a thin flat plate placed parallel to a uniform flow," J. Fluid Mech. **11**, 321 (1961).